Computers and Geotechnics 135 (2021). Submitted 17 Sep 2020; Published 29 April 2021. https://doi.org/10.1016/j.compgeo.2021.104099.

BS-CLAY1: Anisotropic bounding surface constitutive model for natural clays

Mohammad Rezania[1] and Hesam Dejaloud[2]

Abstract

In this paper, a multi-surface anisotropic constitutive model is proposed for clayey soils, based on bounding surface theory and a classical anisotropic critical state-based model. In the proposed model, in addition to volumetric hardening law, rotational hardening rule is also incorporated into the bounding surface formulation with a non-associated flow rule. The model uses the bounding surface plasticity theory to produce a more realistic representation of the nonlinear behavior of clays with high overconsolidation ratios. The detailed model formulation is presented including an innovative approach for finding image stress points on the bounding surface which offers an original conception of changing the projection center even at the absence of plastic loading. Moreover, a modification procedure is discussed to improve the performance of the proposed model for simulating the highly overconsolidated clays. The proposed modifications besides the novel mapping rule form a novel framework that improves the simulation capabilities of the models with elliptical yield/bounding surfaces, particularly in the case of highly overconsolidated clays, and is applicable to all constitutive models with elliptical yield/bounding surfaces. Furthermore, the efficiency of the framework is

[1] Associate Professor, School of Engineering, University of Warwick, Coventry, UK. (Corresponding Author)
Email: m.rezania@warwick.ac.uk. ORCID: https://orcid.org/0000-0003-3851-2442

[2] PhD student, School of Engineering, University of Warwick, Coventry, UK.
Email: hesam.dejaloud@warwick.ac.uk.

demonstrated by comparing the simulation results against element test data from a number of different clays at lightly to highly overconsolidated conditions. The new model shows promising capability in capturing important aspects of natural clays response during straining, in particular the combined effects of small strain nonlinearity with fabric orientation.

1. Introduction

The modified Cam-clay (MCC) model (Roscoe and Burland, 1968) is one of the early constitutive models developed within the critical state soil mechanics (CSSM) framework to enhance the prediction of soft soils behavior, and hence improve the reliability of geotechnical design on soils. An ellipsoid yield surface (YS) was adopted for this isotropic elastoplastic model, and using an associated flow rule it has been able to reasonably replicate many of experimentally observed responses of soft clays. However, natural clay is an intrinsically anisotropic material; this anisotropy may be due to (1) the original structure of the soil fabric (structural anisotropy), (2) the initial stress conditions (inherent anisotropy), and/or (3) the current stress conditions of the soil (stress-induced anisotropy). Furthermore, there are significant amounts of bonding among soil particles that form their natural structure, the degradation and erasure of these bonds during straining strongly influence on their overall behavior. Additionally, MCC assumes a purely linear elastic behavior within the YS. Such an assumption infers an abrupt transition from elastic to plastic strains which is contradictory to experimental observations. Using such a simplistic isotropic elastoplastic constitutive model for practical applications is associated with a number of unrealistic initial assumptions which can result in inaccurate modeling results.

It is a well-established fact that the yield points obtained from tests on undisturbed specimens of natural clay constitute yield surfaces that are inclined in the representative stress spaces. This inclination of the yield surfaces is largely agreed to be due to the inherent fabric anisotropy that exists in the structure of the clay (Dafalias, 1986a; Graham et al., 1983; Nishimura et al., 2007; Wheeler et al., 1999). Given the above, a popular approach in considering the effects of soil anisotropy within a modeling framework has been the development of elastoplastic soil constitutive models that involve inclined yield curves (Sivasithamparam and Rezania, 2017). This methodology for representing the inherent anisotropy has its roots in the works of Sekiguchi (1977) and Hashiguchi (1977) and was subsequently followed by other researchers such as Banerjee and Yousif (1986), Anandarajah and Dafalias (1986), Dafalias (1986a), Whittle and Kavvadas (1994), Ling et al. (2002), Wheeler et al. (2003), Dafalias et al. (2006), Jiang et al. (2012), Karstunen et al. (2013), Rezania et al. (2014), Yang et al. (2015a, b), Sivasithamparam and Castro (2016), Karstunen et al. (2015), Coombs (2017), Nieto Leal et al. (2018), Rezania et al. (2017a, b), Rezania et al. (2018), Chen and Yang (2020). In these works, the rotated YS is either fixed (Sekiguchi & Ohta, 1977; Zhou et al., 2005) or it can change its inclination by adopting a rotational hardening (RH) rule to simulate the development or erasure of anisotropy during plastic straining (Chen and Yang, 2020; Dafalias et al., 2020; Dafalias and Taiebat, 2014; Dafalias and Taiebat, 2013; Dafalias et al., 2006; Wheeler et al., 2003; Yang et al., 2015a, b)

S-CLAY1 model (Wheeler et al., 2003) is an extension of the MCC model with an inclined YS and a simple RH rule to simulate the anisotropic response of soft clays at large plastic strains. Unlike most of the present anisotropic models with an inclined YS where RH rule is only related to plastic volumetric strains (Dafalias and Taiebat, 2014; Dafalias and Taiebat, 2013; Dafalias et al., 2006; Ling et al., 2002) or plastic deviatoric strains (Chen and Yang, 2020), in S-CLAY1 the RH rule is related to both plastic volumetric strains and the plastic shear strains. Some of the main advantages of this model are its relatively simple formulation, realistic K_0 prediction, and simple determination of model parameters values from standard laboratory tests (Rezania et al., 2016), and due to the RH rule formulation, the uniqueness of

Computers and Geotechnics 135 (2021). Submitted 17 Sep 2020; Published 29 April 2021. https://doi.org/10.1016/j.compgeo.2021.104099.

the critical state line (CSL) is preserved (Dafalias and Taiebat, 2013). This model is intended for use with normally consolidated (NC) to lightly overconsolidated (LOC) soft clays, where even a small increase of stress is likely to cause yielding. Moreover, a number of extensions have branched out from this model. Besides the Creep-SCLAY1 (Sivasithamparam et al., 2015) which was developed to consider creep behavior of natural clays and E-SCLAY1S (Sivasithamparam and Castro, 2016) with a new YS based on the framework of logarithmic contractancy, S-CLAY1S (Yildiz et al., 2009) is the most well-known extension of this basic anisotropic model. While S-CLAY1 can capture the effects of plastic anisotropy, it is not applicable for the analysis of natural clays that exhibit a considerable degree of structural sensitivity. For an accurate prediction of the responses of structured sensitive clays, within the constitutive model framework, the effects of bonding and loading-induced destructuration must be taken into account. Using the concept of intrinsic yield surface (Gens and Nova, 1993) because of its practical simplicity, Karstunen et al. (2005) extended the S-CLAY1 model to S-CLAY1S to allow for the effects of soil structure. In the new model, the effect of the initial structure is represented by the difference between the size of the YS of the natural soil and the size of the YS when all of the internal structure/bonding of the soil is destroyed (i.e., the intrinsic YS). In this model, an additional hardening law has been considered to describe the destructuration evolution with plastic straining. However, similar to most classical elastoplastic models, S-CLAY1S only returns elastic strains for the stress states inside the YS which, like its simpler preceding version, restricts its application to simulation of the responses of NC to LOC natural clays under monotonic loading conditions.

To allow for plastic strains at stress states within the YS, different theories have been proposed. The bounding surface (BS) concept is one of the theories which has been widely used to model nonlinear kinematic hardening (Ottosen and Ristinmaa, 2005). This concept was first proposed simultaneously by Dafalias and Popov (1975, 1976) and Krieg (1975) for simulation of cyclic behavior of metals, and was later extended to geomaterials by Anandarajah and Dafalias (1986), Dafalias and Herrmann (1986) and Dafalias (1986b). A detailed description of the mathematical formulation and application of BS plasticity theory in isotropic and anisotropic constitutive models are provided in the abovementioned works. Based on the BS concept, the classical YS can be replaced with a BS on which the actual stress points are mapped to as imaginary stress points. The distance between the real stress points and their corresponding so-called image points are used for the evaluation of the plastic moduli of the actual stress states. To map the real stress points onto the BS, a projection center (PC) is needed. Different methods have been employed to set the location of the PC. Dafalias and Herrmann (1986) considered it to be along the induced hydrostatic line, Whittle and Kavvadas (1994) and Crouch et al. (1994) set PC at the origin of the stress space and Ling et al. (2002) assumed it to be along the K_0 line. Nevertheless, due to its relative simplicity and attractive features, the BS methodology has been rather popular among soil modelers to develop new or extended soil constitutive models (e.g. Chakraborty et al., 2013; Seidalinov and Taiebat, 2014).

In the present work, the BS theory is used to further extend the S-CLAY1 model resulting in a new soil constitutive model which is named the modified BS-CLAY1. The layout of the paper is as follows. In Section 2, the general formulation of the proposed model and its associated hardening rules, plastic modulus, and mapping rule are discussed. Also, in this section, a simplified and a modified approach to specify the PC for the new model are proposed and examined. The disadvantages associated with elliptical BS for simulating the highly overconsolidated (HOC) samples is discussed in Section 3, and as solutions, two modifications are presented and discussed. Section 4 describes the numerical implementation of the model. To determine the effect of model parameters on the model predictions, sensitivity analyses are performed in Section 5. In the following section, the model performance is verified against the test data of a number of clays including kaolin clay, Lower Cromer till, and Boston blue clay. Finally, a concise conclusion is provided in Section 7.

2. Model formulation

BS-CLAY1 is an extension of the S-CLAY1 model which can capture the nonlinearities in the elastic domain while it also accounts for fabric anisotropy of natural clays. The new model employs the same elastic formulation and hardening rules as in the original model. In the following parts, the main components of the proposed model are presented in the general stress space.

2.1. Bounding and loading surfaces

Bounding and loading surfaces are the two important components of the BS plasticity theory. BS or preconsolidation surface is analogous to the YS in classical plasticity theory and it represents the largest pressure that soil elements have experienced during their loading history. The loading surface, on the other hand, is an imaginary surface that carries the stress state. This surface is identical in shape and always smaller or equal in size to the BS; however, no explicit definition is required for that.

The BS-CLAY1 uses the same YS of the S-CLAY1 model as the BS to facilitate the application of an associated flow rule for determining the plastic strain rate direction. Eq. (1) expresses the BS in the general stress space as

$$F = \frac{3}{2}\bar{s}_{ij}\bar{s}_{ij} - \frac{1}{3}(M^2 - \alpha^2)\left[\bar{p}_m' - \frac{1}{3}\bar{\sigma}_{kk}\right]\bar{\sigma}_{kk} = 0 \tag{1}$$

in which

$$\bar{s}_{ij} = \bar{\sigma}_{ij}^{d} - \frac{1}{3}\alpha_{ij}^{d}\bar{\sigma}_{kk} \tag{2}$$

where $\bar{\sigma}_{ij}^{d}$ is the deviatoric stress tensor ($^{-}$ sign denotes the association of the variable to the BS), and α_{ij}^{d} is the deviatoric fabric tensor with the same form as the deviatoric stress tensor. $\bar{p}_m'$ represents the size of BS for the natural clay that represents the maximum pressure that the soil sample has experienced in the past (i.e. preconsolidation pressure). M is the critical stress ratio in compression and scalar $\alpha = \sqrt{(3/2)\alpha_{ij}^{d}\alpha_{ij}^{d}}$. Fig. 1 shows the schematics of the bounding and loading surfaces of the BS-CLAY1 model in the triaxial stress space. In this figure, IS and SS refer to an image stress point and stress state, respectively.

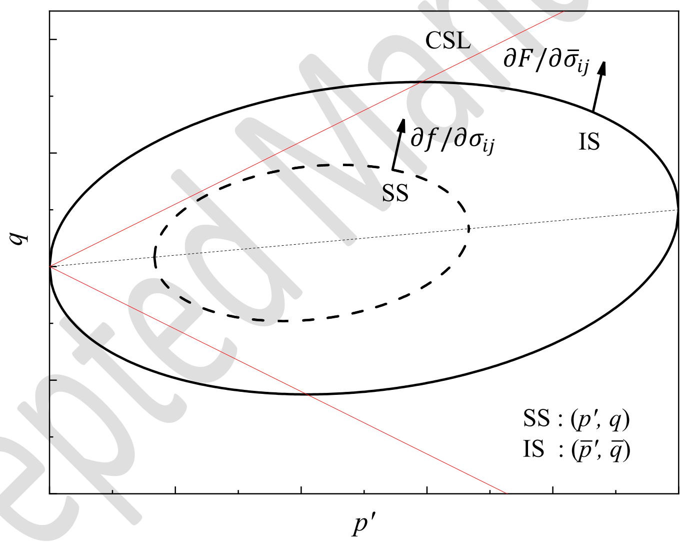

Fig. 1. Schematics of bounding and loading surfaces in BS-CLAY1 model

2.2. Hardening rules

The new anisotropic BS model adopts isotropic and rotational hardening rules similar to those of the S-CLAY1 model to represent any changes in the size and the inclination of the BS due to plastic volumetric and shear strains. It should be noted that no hardening rule is assigned to the loading surface, and it is formed in a way that represents the stress state and changes by stress increments.

Computers and Geotechnics 135 (2021). Submitted 17 Sep 2020; Published 29 April 2021. https://doi.org/10.1016/j.compgeo.2021.104099.

2.2.1. Isotropic hardening rule

For the expansion of the BS, the model adopts an isotropic hardening rule with the same general formulation of that of the MCC model where the changes in the size of the BS are related to the plastic volumetric strain increments, $d\varepsilon_v^p$, as

$$d\bar{p}'_m = \frac{v\bar{p}'_m}{\lambda - \kappa}\, d\varepsilon_v^p \tag{3}$$

in which v is the specific volume, and λ and κ are the slopes of the normal compression and swelling lines in the $(\ln p' - v)$ space, respectively.

2.2.2. Rotational hardening rule

As stated above, the proposed model belongs to the class of anisotropic models where anisotropy is introduced through the initial inclination of the YS (BS in this case) and the kinematic hardening of BS, in terms of its change of inclination during large straining, is captured using an RH rule. In this work, an RH rule, similar to that of the S-CLAY1 model, is employed to describe the rotation of the BS due to the anisotropy. The RH formulation represents the development and erasure of anisotropy due to both plastic volumetric and shear strain increments. In the general stress space, this hardening rule has the form

$$d\alpha_{ij}^d = \mu\left(\left[\frac{3\bar{\sigma}_{ij}^d}{4\bar{p}'} - \alpha_{ij}^d\right]\langle d\varepsilon_v^p\rangle + \beta\left[\frac{\bar{\sigma}_{ij}^d}{3\bar{p}'} - \alpha_{ij}^d\right] d\varepsilon_d^p\right) \tag{4}$$

in which $d\varepsilon_d^p$ is the increment of plastic deviatoric strain. The RH rule has two soil constants, μ and β, where the first one controls the absolute rate at which the deviatoric fabric tensor approaches toward its current target value and the latter controls the relative effect of $d\varepsilon_d^p$ and $d\varepsilon_v^p$ in rotating the BS. Macaulay brackets $< >$ are used so that only the positive $d\varepsilon_v^p$ values are taken into account. The RH formulation of Eq. (4) has been argued not to prevent the excessive rotation of the YS for numerical simulations where stress ratio (η) is significantly higher than the critical stress ratio (Dafalias and Taiebat, 2013); however, it has been proven to be practical for common loading applications (e.g., Rezania et al. (2017a, b) and Karstunen et al. (2015)) and hence adopted in this work in order to keep the developed model within the hierarchical extension of the basic model.

2.3. Plastic modulus of the bounding surface

At this stage of the model development, the associated flow rule is adopted for the BS-CLAY1 model It means that the BS also represents the plastic potential function (i.e., $G = F$). However, in section 3 adoption of the non-associated flow rule in the model is also considered, and the corresponding improved model performance for the HOC samples are discussed. Accordingly, the plastic strain increment is determined as

$$d\varepsilon_{ij}^{p} = \langle L \rangle \frac{\partial G}{\partial \bar{\sigma}_{ij}} \tag{5}$$

where L is the plastic loading index defined as

$$L = \frac{1}{\bar{K}_p} \frac{\partial F}{\partial \bar{\sigma}_{ij}} d\bar{\sigma}_{ij} = \frac{D_{klrs} \frac{\partial F}{\partial \bar{\sigma}_{rs}} d\varepsilon_{kl}}{\bar{K}_p + \frac{\partial F}{\partial \bar{\sigma}_{ab}} D_{abcd} \frac{\partial G}{\partial \bar{\sigma}_{cd}}} \tag{6}$$

in which $\bar{K}_p$ is the plastic modulus of the BS and D_{klrs} is elastic stiffness tensor. To determine $\bar{K}_p$ and establish a complete stress-strain relationship, the consistency condition should be satisfied over the BS. This guarantees that the stress state remains on the BS during plastic flow. Following a standard differentiation of the BS function (i.e., Eq. (1)) with regards to its state variables, the mathematical expression obtained from consistency condition reads as

$$dF = \frac{\partial F}{\partial \bar{\sigma}_{ij}} d\bar{\sigma}_{ij} + \frac{\partial F}{\partial \alpha_{ij}^{d}} d\alpha_{ij}^{d} + \frac{\partial F}{\partial \bar{p}'_m} \frac{d\bar{p}'_m}{d\varepsilon_v^p} d\varepsilon_v^p = 0 \tag{7}$$

Substituting the hardening rules and loading index into Eq. (7), the plastic modulus of the BS is obtained as (refer to the Appendix for more details on the derivation procedure)

$$\bar{K}_p = -\frac{\partial F}{\partial \alpha_{ij}^{d}} \left(\frac{\partial \alpha_{ij}^{d}}{\partial \varepsilon_v^p} \left\langle \frac{\partial G}{\partial \bar{p}'} \right\rangle + \frac{\partial \alpha_{ij}^{d}}{\partial \varepsilon_d^p} \sqrt{\frac{2}{3} \frac{\partial G}{\partial \bar{\sigma}_{ij}^{d}} \frac{\partial G}{\partial \bar{\sigma}_{ij}^{d}}} \right) - \frac{\partial F}{\partial \bar{p}'_m} \frac{\nu \bar{p}'_m}{\lambda - \kappa} \frac{\partial G}{\partial \bar{p}'} \tag{8}$$

2.4. Mapping rule

In the constitutive models modified with BS plasticity theory, the plastic modulus of the actual stress state on the loading surface, K_p, is related to plastic modulus of the image stress point on the bounding surface. Therefore, the plastic moduli of these two points are related to each other through sets of equations called shape hardening functions. In this work, a radial mapping rule is adopted to project the current stress state to an image stress point on the bounding surface.

$$K_p = \bar{K}_p + S_l \tag{9}$$

The shape hardening function, S_l, is defined as

$$S_l = \bar{p}'^{\,3}_m h_l \times \frac{(1 - \rho^{\psi_1})}{\rho^{\psi_2}} \tag{10}$$

where S_l represents the shape hardening function for the loading condition. ψ_1, ψ_2 and h_l are model parameters that control the relationship between loading surface and BS plastic moduli and influence the overall response of the model for the overconsolidated condition. ρ is the ratio of the relative distance of stress state (SS) and projection center (PC) to the relative distance of image stress point (IS) and PC (i.e. $\rho = |\mathrm{SS} - \mathrm{PC}| / |\mathrm{IS} - \mathrm{PC}|$) (see Fig. 2 and Fig.

4). As is clear, when the stress state reaches the BS (i.e. SS = IS), ρ becomes 1, and the hardening shape function value tends to zero.

2.4.1. Projection center

To evaluate ρ, and determine the IS, and calculate the hardening shape function values, first an appropriate PC must be found. In this section, two different methods of finding the PC, which have been tested for the proposed model, are presented and discussed. To this end, the BS is divided into a subcritical side and a supercritical side. The division is from the point at which the CSL intersects the BS. It should be noted that for the development of the mapping rule in the following, if the SS is located to the right of the vertical line passing through the intersection point, it is referred to as a subcritical SS, and otherwise as a supercritical SS.

2.4.1.1. Simple method

For a simplified approach, the PC is assumed to be located at the origin of the stress space and considered to be fixed during the loading procedure. As can be seen in Fig. 2, the loading surface has a fixed point at the origin of the stress space, and its orientation is identical to the BS, but with a different size (p_l). In this case, the following relationship can be used to find the image stress point on the BS from the current SS

$$\bar{\sigma}_{ij} = \frac{1}{\rho} \times \sigma_{ij} \tag{11}$$

Computers and Geotechnics 135 (2021). Submitted 17 Sep 2020; Published 29 April 2021. https://doi.org/10.1016/j.compgeo.2021.104099.

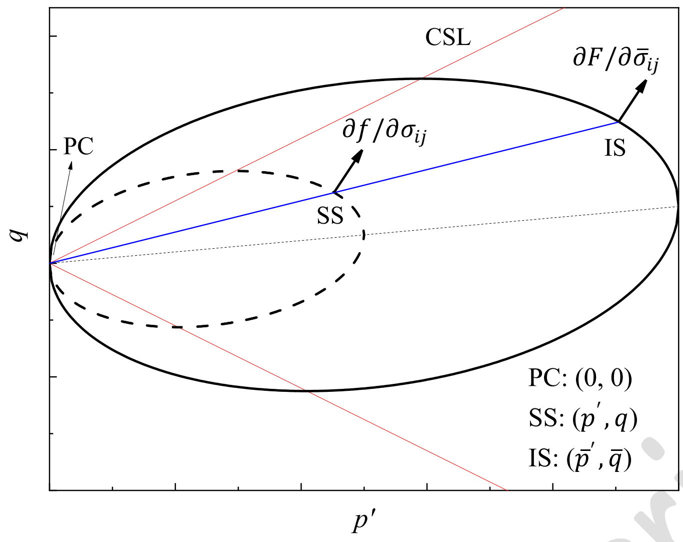

Fig. 2. Schematics of BS-CLAY1 model with projection center located at the origin of stress space

Hence in this approach ρ becomes the similarity ratio between bounding and loading surfaces, and it is identical to the ratio of the size of loading surface to the size of the bounding surface ($p'_l/\bar{p}'_m$). This simplified method is, therefore, an uncomplicated procedure for enhancing a single YS constitutive model with the BS plasticity theory. However, in this method, the accuracy and consistency of the results with the experimental observations are affected by increasing the overconsolidation ratio (OCR) of the soil. For instance, as illustrated in Fig. 3a, for an incremental undrained shearing of a LOC soil specimen, all of the SSs are located in the subcritical side of the BS and their corresponding ISs are also mapped onto this side of the BS. Therefore, based on the BS framework for such an undrained shearing scenario when all stress states, e.g., SS_1, SS_2, and SS_3, are located in the subcritical side, the stress path will continuously incline to the left toward the critical state that is, in fact, the expected response according to the experimental observations. However, for similar loading of a HOC soil, the SSs will be located on the supercritical side of the BS and consequently, as explained in the sequel, the simplified BS procedure will not result in an elegant stress path simulation. For example, if the undrained shearing of a stiff clay is considered (see Fig. 3b), following the simplified method the ISs corresponding to SS_1 and SS_2 are projected to the subcritical side, and the stress state SS_3 is projected to the supercritical side of the BS. In fact, in this scenario following the simplified method, the CSL acts as a dividing line. That is, all the SSs that are located under the CSL are projected to the subcritical side and the SSs located over the CSL will be projected to the supercritical side of the BS. This will cause the stress path to initially tend to the left and then incline to the right when it crosses the CSL. Such behavior is not observed in experimental studies on HOC clays where the undrained shearing stress path is inclined to the right continuously from the beginning of loading. This implies that some modifications in the definition of PC are required. In the following section, a modified method is proposed and discussed.

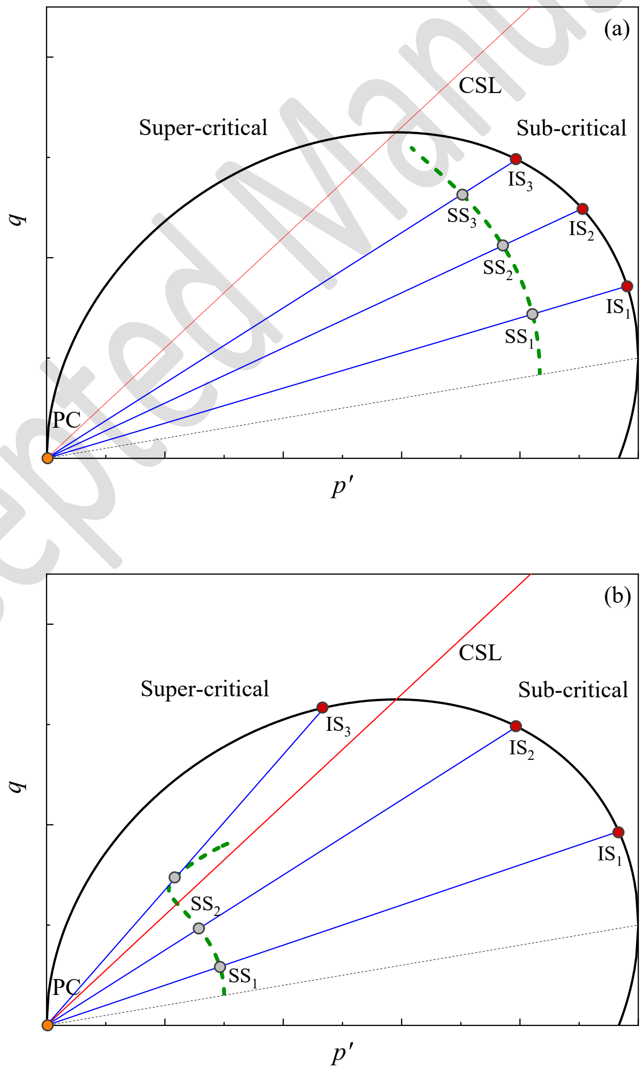

Fig. 3. Simulation of stress paths for (a) LOC (b) HOC clay with the simplified method

2.4.1.2. Modified method

To resolve the pitfall of using the simplified method, in this work a number of different rules for defining the PC have been examined. From the analyses, it was found that in order to consistently better predict the experimentally observed loading paths in both LOC (i.e., soft) and HOC (i.e., stiff) domains, the PC should be defined in such a way that the subcritical SSs are projected to the subcritical side of the BS, and supercritical SSs are projected to the supercritical side of the BS. To achieve this in the modified method, the PC is defined on the α-line and it is assumed that it can freely move within the BS with the variations of the SS. Similar concepts were also used in the literature (Ling et al., 2002; Seidalinov and Taiebat, 2014). By adopting a moving PC, the location of the projection center in the general stress space (σ_{ij}^c) can be readily defined as a fraction of the size of the BS. To this end, using the radial mapping rule the image stresses are related to the actual stresses through

$$\sigma_{ij}^c = \zeta\, \bar{p}'_m \left(\alpha_{ij}^d + \delta_{ij}\right) \tag{12}$$

In this equation, ζ is the parameter which, based on the current SS, changes the location of the PC and is defined as

$$\zeta = \gamma_1 \left(1 - \frac{p'}{\bar{p}'_m}\right) \tag{13}$$

in which γ_1 is the model constant. Substituting Eq. (13) in Eq. (12), the PC is calculated as

$$\sigma_{ij}^c = \gamma_1 \left(\bar{p}'_m - p'\right)\left(\alpha_{ij}^d + \delta_{ij}\right) \tag{14}$$

It must be considered that the PC shall always lay within the BS. Therefore, the parameter γ_1 should be limited to the following value

$$\gamma_{1,max} = \frac{\bar{p}'_m}{\bar{p}'_m - p'} \tag{15}$$

Eq. (14) implies that the location of the PC changes with the variations of SS, BS magnitude, and the degree of anisotropy. That is, contrary to the model proposed by Ling et al. (2002), even when the stress state varies inside the BS and has not intersected with it, the location of the PC can change. Based on the hardening laws used in the proposed model, the variations of PC are defined as

$$\dot{\sigma}^c_{ij} = \gamma_1\gamma_2\left[(\dot{\bar{p}}'_m - \dot{p}')(\alpha^d_{ij} + \delta_{ij}) + (\bar{p}'_m - p')\dot{\alpha}^d_{ij}\right] \tag{16}$$

where γ_2 is applied to control the pace of PC variations. As will be shown in the parameter determination section, this parameter is considered less than 1, and therefore, the condition of being inside the BS is not violated for the PC. If $\gamma_1 = 0$, the PC moves to the origin of the stress space and the modified method turns back into the simplified method, and if γ_2 becomes zero, the PC remains fixed during the loading. To find the location of the IS on the BS, as shown in Fig. 4 for the triaxial stress space, the line passing through the PC and SS intersects with the BS which, depending on the location of SS, one of the two intersection points is selected as the IS. To find the image stress point, the following equations should be satisfied

$$\bar{p}' = \frac{1}{\rho}(p' - p'_c) + p'_c$$

$$\bar{q} = \frac{1}{\rho}(q - q_c) + q_c \tag{17}$$

where the subscript c in p'_c and q_c stands for the projection center. Fig. 5, shows the variations of PC during loading. It should be noted that by considering $\gamma_2 = 1$, the projection center is always located on the α-line and its location varies with the variations of SS; as a result, the stress path is invariably inclined to the right toward the critical state.

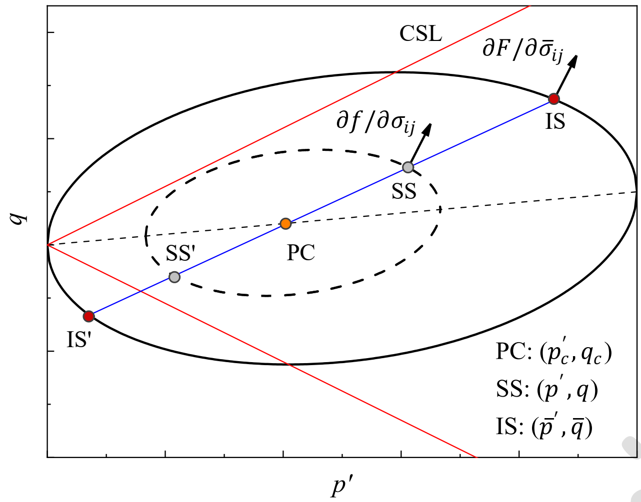

Fig. 4. Schematics of BS-CLAY1 model with modified projection center

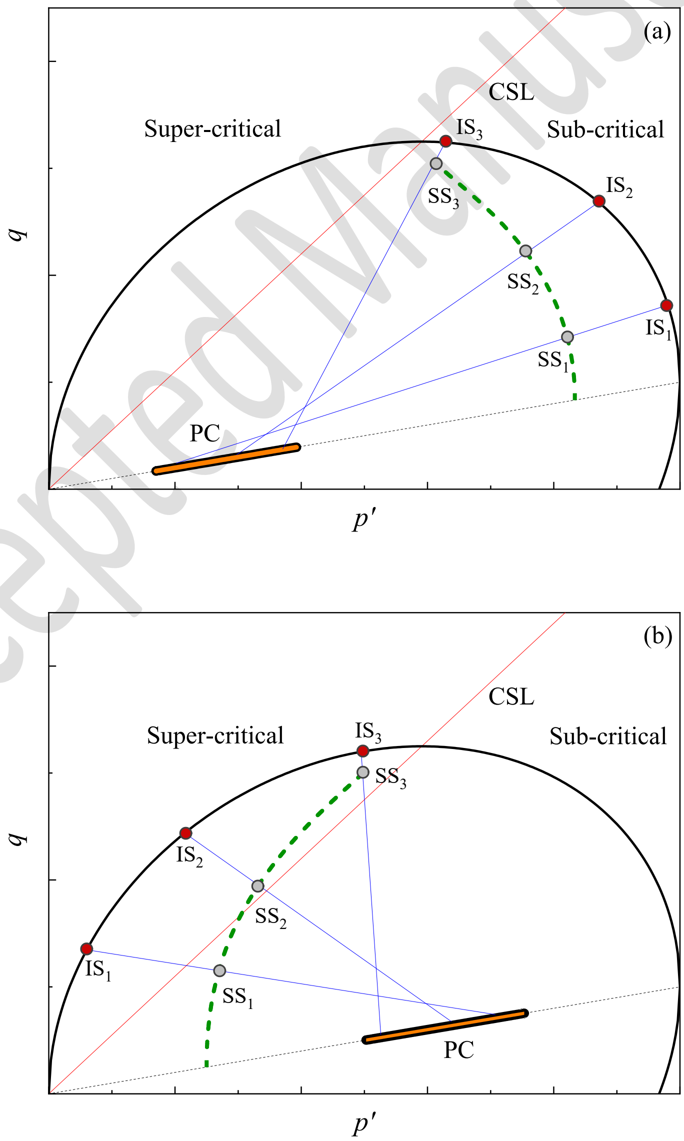

Fig. 5. Simulation of stress paths for (a) LOC (b) HOC clay using modified projection method

3. Discussion on the elliptical bounding surface deficiencies – problem statement

Although elliptical BSs provide acceptable predictions for NC and LOC clays with low computational efforts, they are almost unable to properly simulate the behavior of HOC samples properly. Since the BS theory enables the constitutive models to capture the nonlinear behavior inside the BS, it cannot modify the peak strength associated with the bulky shape of elliptical BSs. Therefore, there might be a significant deviation between simulated shear strength and test data, and this divergence can be more notable with increasing the OCR. It is noteworthy that in some cases, the bounding surface theory intensifies this discrepancy, especially for OCR > 2. To address this, Fig. 6 demonstrates the comparison of stress paths predicted by S-CLAY1 and BS-CLAY1 for an isotropically consolidated sample of Lower Cromer till (Gens, 1982) with OCR = 4 (Table 1). As can be seen, the simulated stress path by S-CLAY1 goes up vertically until it touches the yield surface, and then it changes its direction toward the CSL due to softening and the RH rule makes it to follow the CSL until the inclination of the BS reaches the equilibrium value of anisotropy. However, the BS-CLAY1 reproduces a nonlinear stress path that passes the CSL and tends to reach the CSL at higher deviatoric stresses without touching the BS. Since the BS has a bulky elliptical shape, there is considerable room for the stress path to continue its increments without triggering plastic hardening rules. The overestimated peak shear strength of HOC clays besides the unsatisfactory performance in capturing the yield points convinced researchers to use yield surfaces with different shapes, i.e. teardrop-shaped surfaces (Chen and Yang, 2017; Chen and Yang, 2020; Collins and Kelly, 2002; Collins and Hilder, 2002; Lagioia et al., 1996; Taiebat and Dafalias, 2010). Since the S-CLAY1 employs an elliptical YS and modifying the shape of the YS is out of the scope of this paper, possible solutions for improving the estimation of the peak shear strength of HOC samples are presented in the subsequent sections.

Computers and Geotechnics 135 (2021). Submitted 17 Sep 2020; Published 29 April 2021. https://doi.org/10.1016/j.compgeo.2021.104099.

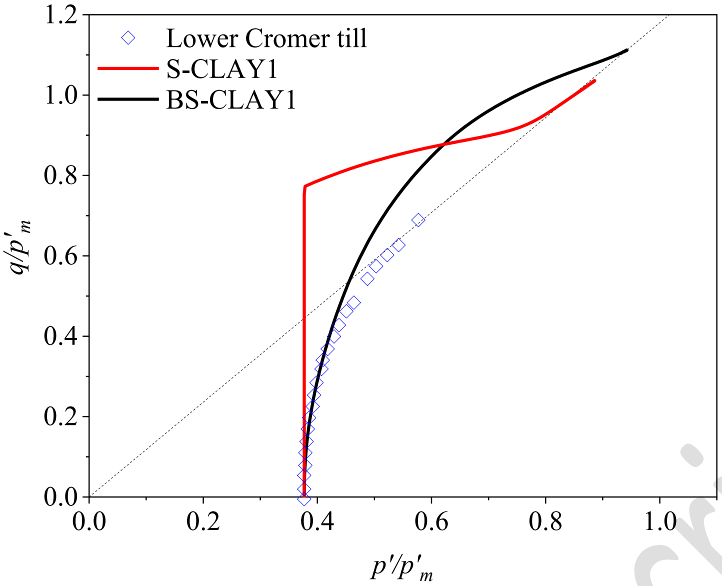

Fig. 6. Comparison of S-CLAY1 and BS-CLAY1 for undrained triaxial test on HOC sample

3.1. Problem solutions

In order to improve the prediction of peak strength of HOC samples, a step-by-step procedure is taken into account. In the first step, a non-associated flow rule is adopted to the proposed model. This stage is followed by introducing modified hardening rules that are used while the stress state is located inside the BS. In each step, the effect of the modifications is illustrated using a comparison of simulated stress paths with the experimental data result of an undrained triaxial test on the sample of Lower Cromer till.

3.1.1. Non-associated flow rule

Although some studies (Yu, 1998; Jiang and Ling, 2010; Jiang et al., 2012) suggest that using associated flow rule is a feasible assumption for constitutive models with an oriented YS, it was found that employing non-associated flow rule leads to more realistic simulations (Yu, 1998). In the case of the HOC clays, the non-associated flow rule provides the opportunity to define slender BS to shrink the elastic domain. In addition to improving the simulation capabilities for NC samples, this contraction helps the stress path to reach to CSL at lower deviatoric stress, and it relatively modifies the overestimated peak strength.

Computers and Geotechnics 135 (2021). Submitted 17 Sep 2020; Published 29 April 2021. https://doi.org/10.1016/j.compgeo.2021.104099.

314 To establish the non-associated flow rule formulation, the BS in Eq. 1 should be rewritten
315 in the following form

$$F = \frac{3}{2}\bar{s}_{ij}\bar{s}_{ij} - \frac{1}{3}(N^2 - \alpha^2)\left[\bar{p}'_m - \frac{1}{3}\bar{\sigma}_{kk}\right]\bar{\sigma}_{kk} = 0 \tag{18}$$

316 where the M is replaced with a constant yield surface shape factor, N. A similar oriented and
317 sheared elliptical surface with different size is also used for the plastic potential surface (PPS)

$$G = \frac{3}{2}\bar{s}_{ij}\bar{s}_{ij} - \frac{1}{3}(M^2 - \beta^2)\left[\bar{p}'_g - \frac{1}{3}\bar{\sigma}_{kk}\right]\bar{\sigma}_{kk} = 0 \tag{19}$$

318 where β and $\bar{p}'_g$ represent the inclination and the size of the PPS, respectively. The proposed
319 model does not employ any rotational hardening rule for the plastic potential surface, and it
320 assumes an identical inclination for the BS and the PPS ($\alpha = \beta$).

321 Fig. 7a shows the effect of considering the non-associated flow rule on the response of the
322 model in simulating the behavior of HOC clay. As can be seen, although employing the non-
323 associated flow rule has a significant impact on model performance and the peak strength
324 estimation, the model needs more modifications to reproduce more accurate predictions.

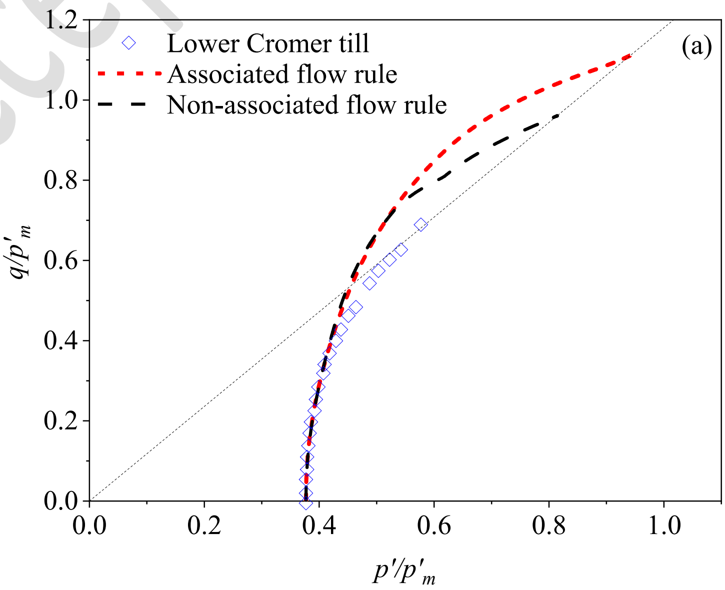

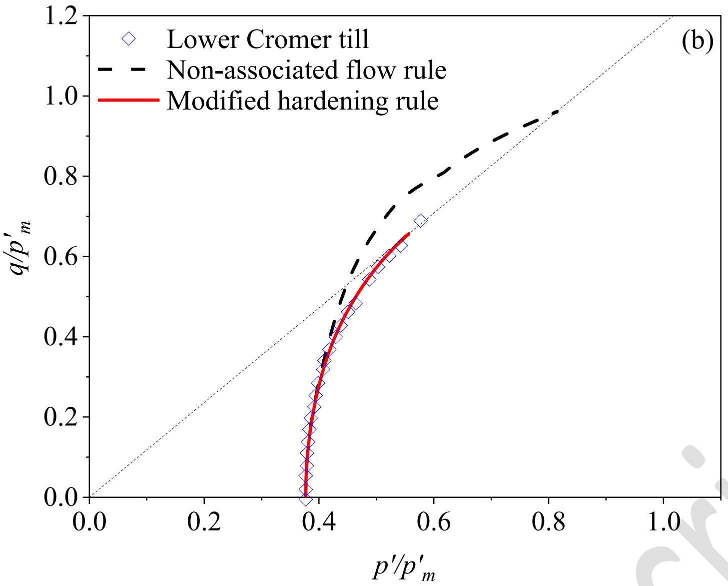

Fig. 7. Effects of modifications on the model response, (a) effect of non-associated flow rule, and (b) modified hardening rule

3.1.2. Modified hardening rules

The main idea of this modification is to change the size and inclination of the BS while the SS varies inside the BS. This variation should be such that the SS of the HOC sample touches the BS sooner. To this end, specific hardening rules are adopted to the model which drag the BS towards the SS for HOC samples and virtually tighten the elastic domain. Therefore, the following modified hardening rules are defined to adjust the BS based on the plastic strain increments that are determined using the gradients of BS and PPS at the IS and the plastic modulus of the current SS, (K_p)

$$d\bar{p}'_m = A\left(\frac{\bar{p}'_m}{p'}\right)^2 \frac{v\bar{p}'_m}{\lambda - \kappa}\, d\varepsilon_v^p \tag{20}$$

$$d\alpha_{ij}^d = A\left(\frac{\bar{p}'_m}{p'}\right)^2 \mu\left(\left[\frac{3\bar{\sigma}_{ij}^d}{4\bar{p}'} - \alpha_{ij}^d\right]\langle d\varepsilon_v^p\rangle + \beta\left[\frac{\bar{\sigma}_{ij}^d}{3\bar{p}'} - \alpha_{ij}^d\right] d\varepsilon_d^p\right) \tag{21}$$

$$A = \frac{< OCR - 2 >}{OCR - 2} = \begin{cases} 1 & OCR > 2 \\ 0 & OCR \leq 2 \end{cases} \tag{22}$$

which the term $\left(\frac{\bar{p}'_m}{p'}\right)^2$ is considered to amplify the effect of modified hardening rules with increasing the OCR, and A is a constant parameter that vanishes the modified hardening rule for $OCR \leq 2$. As the modified mapping rule projects the IS on the dry side of the CSL, the modified hardening rules reproduce softening-like behavior associated with HOC samples.

Fig. 7b shows the effect of using both non-associated flow rule and modified hardening rule on the model simulations. As can be seen, the modified hardening rule improves the predictions significantly, and the model response fits very well with experimental data. Although the most logical way to capture the peak shear strength of HOC samples more accurately is using the teardrop-shaped yield/bounding surface, using the proposed modified hardening rules associated with BS theory and proper mapping rule can enhance the elliptical BS to replicate the peak strength with the desired accuracy level.

4. Numerical implementation

In this implementation, the plastic strain components associated with the BS evolution can be obtained using the Euler backward implicit integration scheme. For this purpose, the plastic multiplier or plastic loading index (Eq. 6) can be rewritten in terms of BS value as

$$L = \frac{F}{\bar{K}_p + \frac{\partial F}{\partial \bar{\sigma}_{ij}} D_{ijkl} \frac{\partial G}{\partial \bar{\sigma}_{kl}}} \tag{23}$$

Using the Euler backward implicit integration scheme, the occurrence of plastic strains is guaranteed while the prescribed convergence criterion for the iterative stress integration with respect to the BS is satisfied (i.e. $F < 10^{-7}$). Under this condition, the trial stress in step $(n+1)$ can be obtained from stresses at the previous step (i.e., step n) as follow

Computers and Geotechnics 135 (2021). Submitted 17 Sep 2020; Published 29 April 2021. https://doi.org/10.1016/j.compgeo.2021.104099.

$$\sigma_{ij}^{(n+1)} = \sigma_{ij}^{(n)} + d\sigma_{ij} \tag{24}$$

where the stress increment is calculated as

$$d\sigma_{ij} = D_{ijkl} d\varepsilon_{kl}^{e} = D_{ijkl}(d\varepsilon_{kl} - L\, D_{klmn} \frac{\partial G}{\partial \bar{\sigma}_{mn}}) \tag{25}$$

In order to obtain stable solutions, if necessary, the size of the strain increment can be controlled through sub-stepping. It should be noted that for the stress states inside the BS, an explicit Euler Forward integration scheme is employed for the stress integration. A summary of the implementation algorithm for the proposed model is presented in Fig. 8.

READ: Initial stress state(σ_{ij}^{0}), state variables, strain increment($d\varepsilon_{ij}$)
IF (strain increment subdivision is required) THEN
    Determine sub increment number (N_{sub})
    Subdivide strain increment: $d\varepsilon_{ij}^{sub} = d\varepsilon_{ij}/N_{sub}$
END IF

DO n=1, N_{sub}
    Trial strain increment: $d\varepsilon_{ij}^{trial} = d\varepsilon_{ij}^{sub}$
    Convergence criteria: FALSE
    DO WHILE (Not converged)
        Convergence criteria: TRUE
        Image stress point: $\bar{\sigma}_{ij}$
        Plastic modulus of bounding surface: $\bar{K}_p$
        Shape hardening function: S_l
        Plastic modulus of loading surface: $K_p = \bar{K}_p + S_l$
        Explicit plastic loading index (plastic multiplier): L
        Plastic strain increment based on BS and PPS gradient at image stress point: $d\varepsilon_{ij}^{plastic,IS}$
        Elastoplastic stiffness tensor: D_{ijkl}^{ep}
        $d\sigma_{ij}^{trial^{(n)}} = D_{ijkl}^{ep} d\varepsilon_{kl}^{trial^{(n)}}$
        $\sigma_{ij}^{trial^{(n)}} = \sigma_{ij}^{0} + d\sigma_{ij}^{trial^{(n)}}$
        Calculate: Bounding surface value: F
        IF ($F > 10^{-7}$) THEN
            Plastic modulus of bounding surface: $K_p = \bar{K}_p$
            Implicit plastic loading index (plastic multiplier): L
            Plastic strain increment: $d\varepsilon_{ij}^{plastic}$
            Convergence criteria: FALSE
        END IF
        Update stress variable
    END DO
END DO

Fig. 8. Implementation algorithm for the BS-CLAY1

5. Model parameters

The input soil constants and state variables required for the proposed model can be categorized into the following four groups: (1) isotropic parameters including $\bar{p}'_m$, e_0 (initial void ratio), M, N, λ, κ and ν (Poisson's ratio) which are similar to those of the MCC model, (2) anisotropy parameters including α_0 (initial value of α), μ and β, and (3) BS plasticity parameters γ_1, γ_2, h_l, ψ_1, and ψ_2. The evaluation of the isotropic parameters is straightforward and they can be determined from the results of standard geotechnical tests as is the routine for MCC-based critical state models (see, for example, Muir Wood, 1990). The N parameter can be calibrated by both fitting the BS to yield stress points in stress space and by using the experimental data results of the undrained triaxial tests.

In theory, the initial orientation of the clay fabric should be represented in a tensorial form with independent components; however, for practical simplicity, clay's initial fabric orientation is commonly considered to be of cross-anisotropic nature which is a realistic assumption as natural clays have generally been deposited only one-dimensionally in a vertical direction (Rezania et al., 2014; Sivasithamparam and Rezania, 2017). With this assumption, determination of the components of initial fabric tensor is significantly simplified as they can now be computed using a scalar α_0 which represents the initial inclination of the BS. Where enough experimental data are available for yield stress points from triaxial tests under different stress paths, the value of α_0 can be readily calibrated. However, as this is not often the case, it is reasonable to assume that the initial inclination of BS has been developed under K_0 (coefficient of earth pressure at rest) loading, based on this assumption Wheeler et al. (2003) proposed the following closed-form relationships for determination of α_0 and β

$$\alpha_0 = \frac{{\eta_{K_0}}^2 + 3\eta_{K_0} - M^2}{3} \tag{26}$$

and

$$\beta = \frac{3\left(4M^2 - 4{\eta_{K_0}}^2 - 3\eta_{K_0}\right)}{8\left({\eta_{K_0}}^2 - M^2 + 2\eta_{K_0}\right)} \tag{27}$$

where η_{K_0} is the ratio of deviatoric to mean effective stress at K_0 condition (i.e., $\eta_{K_0} = 3(1-K_0)/(1+2K_0)$. The value of K_0 can be measured, or estimated using Jaky's formula for NC soils (i.e., $K_0 \approx 1 - \sin\phi'$, with ϕ' being the soil friction angle at critical state) or Mayne and Kulhawy's (1982) formula for overconsolidated soils (i.e., $K_0 \approx (1 - \sin\phi')OCR^{\sin\phi'}$). Given the dependence of K_0 and M to ϕ' (e.g., $M = 6\sin\phi'/(3-\sin\phi')$, Wheeler et al. (2003) suggested that for NC to LOC soils α_0 and β are uniquely related to ϕ'. However, based on the authors' experience, Eqs. (26) and (27) yield reasonable prediction results for overconsolidated soils, as well. The other anisotropy constant, μ, can be best evaluated by calibrating against experimentally observed data, for example from specialized multi-stage loading-unloading-reloading stress path triaxial tests where different loading stages involve a major change in the stress path direction that facilitates excessive rotation of the BS. As such loadings are not typical in practical conditions, it is safe to assume that model performance is not particularly sensitive to the values of μ; hence, for its determination, calibration against standard isotropic compression test data should suffice. It should be noted that, based on experimental verifications, Wheeler et al. (2003) suggested that the value of β should be between $0.5M$ and M, and Zentar et al. (2002)suggested that the value of μ should normally lie in the range $10/\lambda$ and $15/\lambda$.

The sensitivities of model predictions on the values of BS parameters, h_l, ψ_1, ψ_2, γ_1 and γ_2 are illustrated in Fig. 9. Fig. 9a shows that increasing the parameter h_l clearly influences the behavior predicted by the model for both LOC and HOC conditions. As Fig. 9b shows, changing ψ_1 also makes notable changes on model prediction; however, its effect on the prediction of HOC samples is not as bold as h_l and happens within a smaller range of plausible values. These trends can be explained by looking at Eq. (10) when these parameters' values approach very large numbers, i.e. infinity. For h_l, as its value tends toward infinity the limit of Eq. (10) tends toward infinity too. Hence, the proposed model reduces to a standard elastoplastic model and predicts the soil behavior similar to S-CLAY1. On the other hand, when ψ_1 tends to infinity Eq. (10) results in a value which is a function of h_l and ψ_2 (re-written in Eq. (28)), not necessarily a large number. Fig. 9b shows that as ψ_1 increases, the model shows less sensitivity to its variations.

$$\lim_{\psi_1 \to \infty} S_l = \frac{\bar{p}_m'^{\,3} h_l}{\rho^{\psi_2}} \tag{28}$$

Fig. 9c shows the effects of changing ψ_2 values on model predictions. This parameter, similar to h_l, can cause significant effects on the model response. However, unlike h_l, it can bring the effects of the existence of an elastic core into the model predictions. It can be explained by the limit of Eq. (10) when ψ_2 approach infinity. In this case, the limit of the Eq. (10), first rapidly tends toward infinity and as the loading process progresses and ρ increases, its pace toward infinity decreases. Consequently, for the early parts of the stress path, the predicted behavior resembles that of the standard elastoplastic models, and as ψ_2 continues to increase, the BS effects on model predictions becomes pronounced. The effect of parameter γ_1, for LOC and HOC conditions, is shown in Fig. 9d. As can be seen, when the soil is lightly overconsolidated, γ_1 has negligible effects on the results, while for the HOC soils, the variations of γ_1 have notable effects on the model response. Therefore, this parameter can be used for the calibration of the model at HOC conditions .However, it should be kept in mind that high values of γ_1 can reproduce anomalies, i.e. $\gamma_1 = 1$ in Fig. 9d, due to the improper projected image points and the pace of PC evolutions. Moreover, the main reason for the different model response by considering $\gamma_1 = 0.25$ is that unlike other values of γ_1, this value results in the projection center on the left side of the SS, and hence, the ISs are located on the subcritical side of the BS. Therefore, it is noteworthy that suitable values should be assigned to this parameter based on the OCR values. Fig. 9e shows how the variation of the γ_2 can affect the model simulations slightly. As is clear, γ_2 have an insignificant influence on the model predictions. The main role of this parameter is to control the SS to remain inside the BS during softening behavior associated with newly define modified hardening rules by reducing the pace of PC evolutions (Eqs. 20 and 21).

Although any real positive number can be assigned to shape hardening function parameters (h_l, ψ_1, and ψ_2), the model predictions and sensitivity analysis are evaluated to establish a relationship between them to reduce the model constants without affecting simulation capabilities. Regarding this, as reasonable responses are reproduced using the value of h_l between 10 to 100, the authors suggest considering ψ_1 using the following equation

$$\psi_1 = \frac{h_l}{10} - 1 \tag{29}$$

and choosing ψ_2 between $0.5\psi_1$ to $1.5\psi_1$. A similar assessment procedure is conducted over projection center parameters (γ_1 and γ_2). Since the position of the projection center is directly related to the consolidation stress state and the OCR, attempts to correlate projection center parameters to OCR lead to the following equations

$$\gamma_1 = \frac{2.5}{OCR} \tag{30}$$

$$\gamma_2 = \max\{\frac{2.0}{OCR}, 1\} \tag{31}$$

Computers and Geotechnics 135 (2021). Submitted 17 Sep 2020; Published 29 April 2021.
https://doi.org/10.1016/j.compgeo.2021.104099.

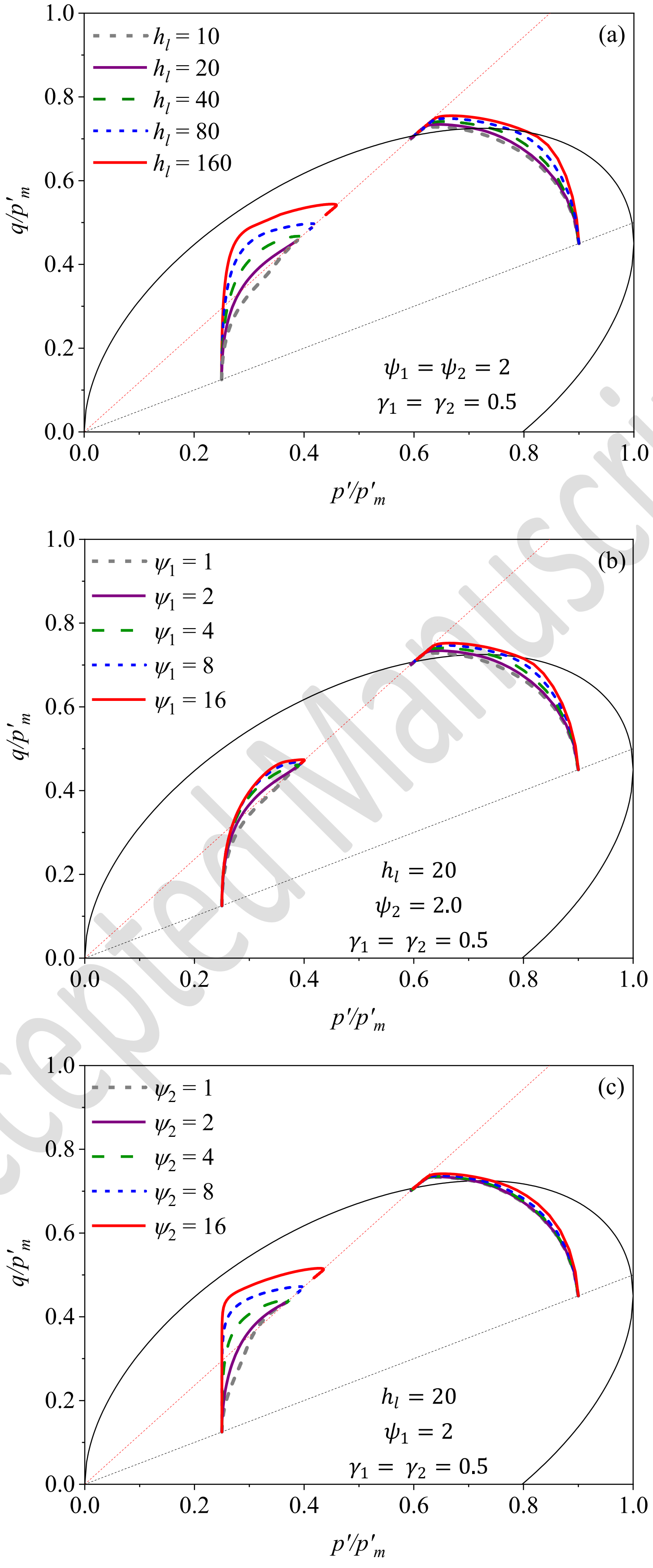

Computers and Geotechnics 135 (2021). Submitted 17 Sep 2020; Published 29 April 2021. https://doi.org/10.1016/j.compgeo.2021.104099.

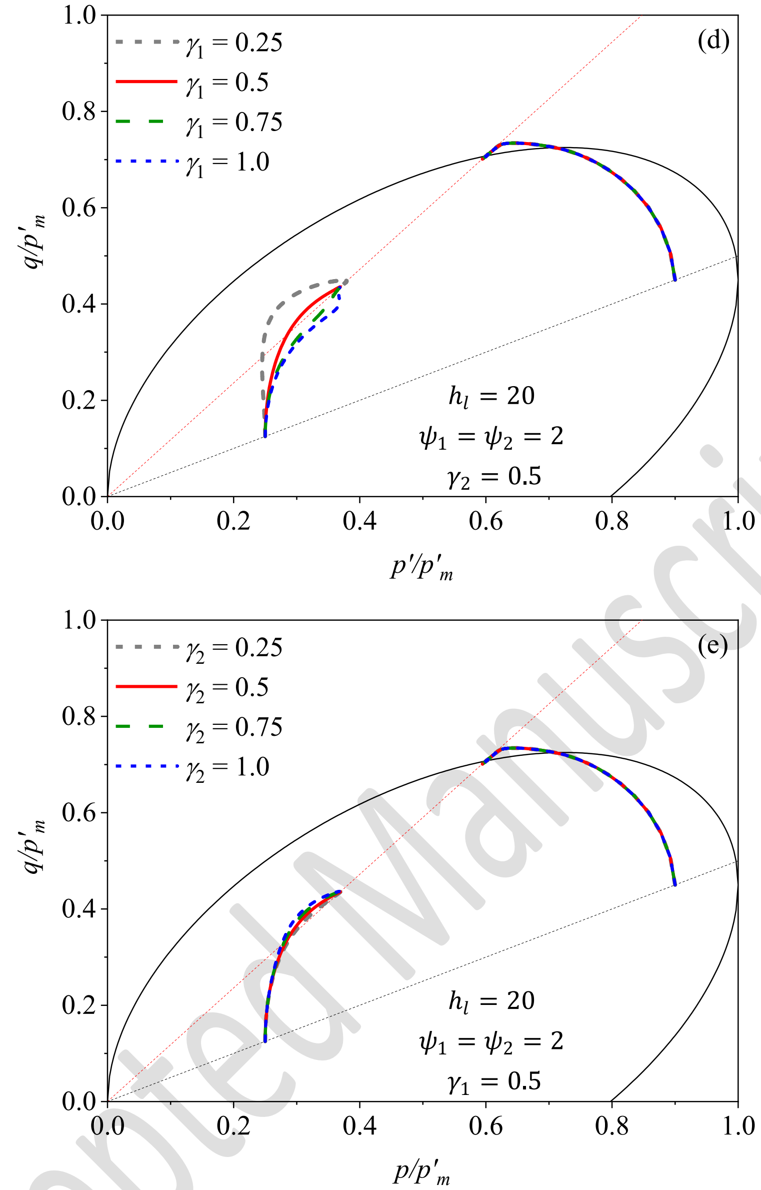

Fig. 9. Model sensitivity analysis with BS parameters: (a) h_l, (b) ψ_1, (c) ψ_2, (d) γ_1, and (e) γ_2

6. Comparison with experimental data

In this section, the numerical performance of the newly proposed anisotropic BS model is verified using available element level experimental data from the literature. To this end, the compression triaxial test data for three different soils including Kaolin Clay (Banerjee et al., 1985), Boston blue clay (Ladd and Varallyay, 1965), and Lower Corner till (Gens, 1982) are used. Prior to the simulations, and following the procedures described in the previous section, the model parameters are first calibrated. For all three soil types, the parameter calibration has begun with the determination of anisotropy parameters using the experiments carried out at

Computers and Geotechnics 135 (2021). Submitted 17 Sep 2020; Published 29 April 2021. https://doi.org/10.1016/j.compgeo.2021.104099.

OCR=1. Then the BS parameters are calibrated at higher OCRs. Table 1 summarizes the model parameter values for each soil type which are further discussed in the following.

Table 1. Initial values of the state variable and constants of the BS-CLAY1 model adopted for three types of clays

Parameter		Kaolin clay	Boston Blue clay	Lower Cromer till
Critical state and yield surface	e_0	0.94–1.07	1	1.79
	ν	0.2	0.227	0.258
	κ	0.05	0.036	0.009
	λ	0.14	0.184	0.63
	N	0.85	0.98	1.03
	M	1.05	1.35	1.18
Anisotropy	α_0	Variable	0.57	0.45
	μ	150	280	260
	β	0.57	0.30	0.74
Bounding surface	γ_1		2.5/OCR	
	γ_2		2.0/OCR	
	h_l	35	30	50
	ψ_1	2.5	2	4
	ψ_2	2.5	2	4

6.1. Kaolin clay

A series of undrained triaxial tests on fully saturated Kaolin clay samples were conducted by Stipho (1978). In his stress-controlled compression experiments on anisotropically consolidated samples (K_0 = 0.8, 0.67, and 0.57), Stipho (1978) considered different OCR values ranging from 1.0 to 4.0. In these experiments, the preconsolidation stress $\bar{p}'_m$ was 204 kPa for anisotropically consolidated samples. The experimentally observed soil responses from these tests are used here to validate the prediction capability of the developed model. It is worth

Computers and Geotechnics 135 (2021). Submitted 17 Sep 2020; Published 29 April 2021. https://doi.org/10.1016/j.compgeo.2021.104099.

mentioning that the initial rotations of the BS for different K_0 values are obtained from Sivasithamparam and Castro (2015) by simulation of the K_0 stress paths.

Fig. 10 shows the simulation results obtained from the BS-CLAY1 model in comparison to the test data. In these figures, the solid lines show the predicted results for compression tests. As can be seen, the BS-CLAY1 model simulations are both qualitatively and quantitatively consistent with the experimentally observed responses in the stress path and the stress-strain spaces. Neglecting the inability of experimental data in capturing the failure properly, due to stress-controlled nature of the tests (Sivasithamparam and Castro, 2015), at HOC conditions (e.g., OCR=4), the simulations of the BS-CLAY1 model fit very well with the test results.

The comparisons for corresponding stress-strain (in terms of normalized deviatoric stress, q/p'_m, versus axial strain, ε_1) are shown in Fig. 10. The performance of the proposed BS-CLAY1 model is remarkably accurate for HOC samples. It correctly predicts a continuously hardening response with no peaks, similar to what was experimentally observed (see, for example, Figs. 10a, c, e).

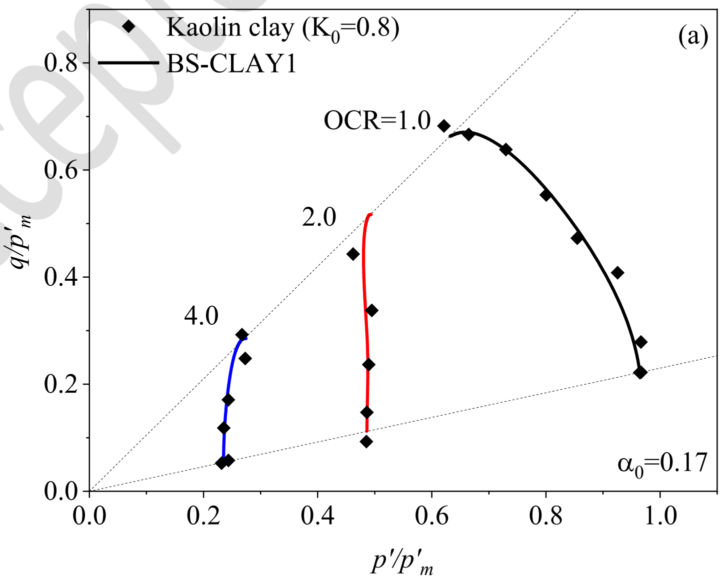

Computers and Geotechnics 135 (2021). Submitted 17 Sep 2020; Published 29 April 2021.
https://doi.org/10.1016/j.compgeo.2021.104099.

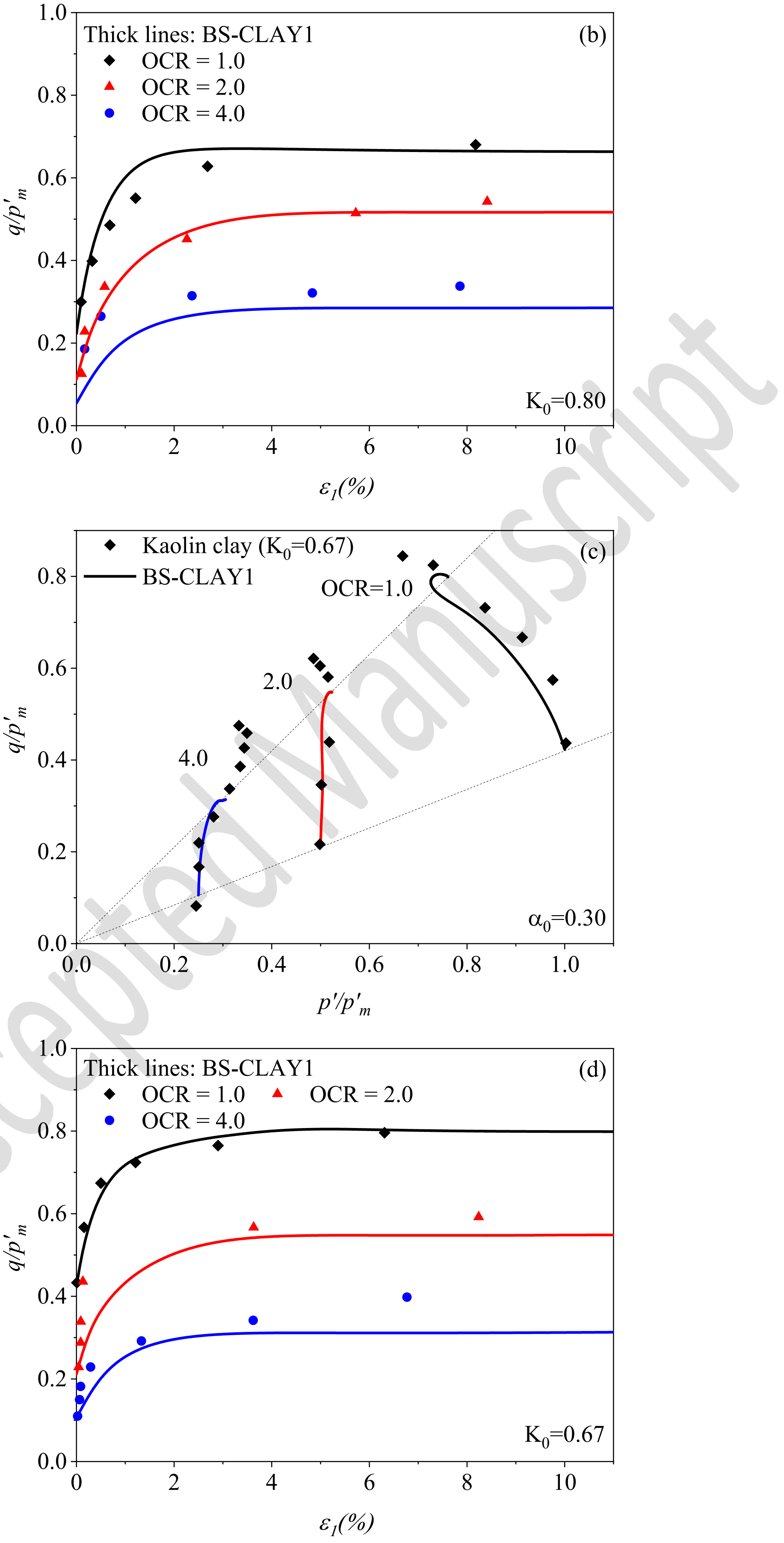

Computers and Geotechnics 135 (2021). Submitted 17 Sep 2020; Published 29 April 2021. https://doi.org/10.1016/j.compgeo.2021.104099.

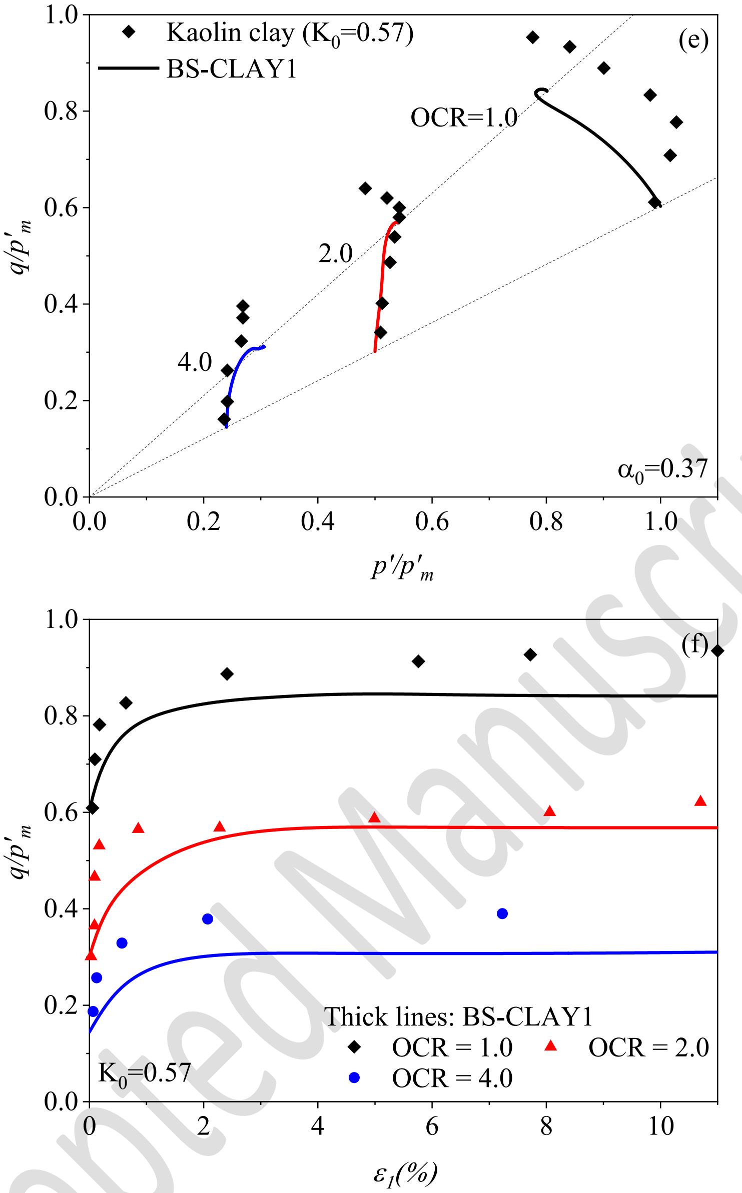

Fig. 10. Comparison of BS-CLAY1 predictions for Kaolin clay

6.2. Boston blue clay

Boston Blue clay is a marine clay type that exists in a layer of the complex Boston soil deposit. The dry and saturated unit weights of this soil are 1826-1922 kg/m^3 and 1281-1393 kg/m^3, respectively. Moreover, the liquid limit, plasticity index, and liquidity index of Boston blue clay are 41%, 21%, and 0.8%, respectively. A series of undrained compression triaxial tests on anisotropically consolidated samples of Boston blue clay were performed by Ladd and Varallyay (1965) and Fayad (1986). The specimens were tested at e_0=0.84–0.89 with p'_m ranging from 273 to 785 kPa. The model parameter values, determined for simulations, are summarized in Table 1 among which the values of conventional critical state parameters are taken from Chen and Yang (2020).

Fig. 11 show the BS-CLAY1 predictions of normalized stress paths and corresponding stress-strain curves for isotropically and anisotropically consolidated samples of Boston blue clay, respectively. Fig. 11a shows that, excluding OCR=2, the stress path predictions are in good agreement with experimental measurements. Moreover, the model responses are promising in stress-strain space, despite the inability of the model to generate softening behavior. Also, the numerical predictions of deviatoric stress (normalized with initial preconsolidation pressure) versus axial strain, shown in Fig. 11b, are in acceptable agreement with the experimental results.

In the case of OCR=2, the model predicts the failure strength properly in the stress-strain space, while it fails to follow the stress path closely. Moreover, introducing the non-associated flow rule does not help the model to simulate the behavior of the NC sample reasonably. Ling et al. (2002) attributed this to the clay's softening behavior and suggested that a kinematic hardening approach may resolve the discrepancies. Since the BS plasticity theory cannot adjust the prediction of the behavior of NC samples, the simulations could be improved by using more sophisticated BSs as well as using a destructuration hardening rule. Employing a more flexible RH rule can also be helpful in generating more precise simulations.

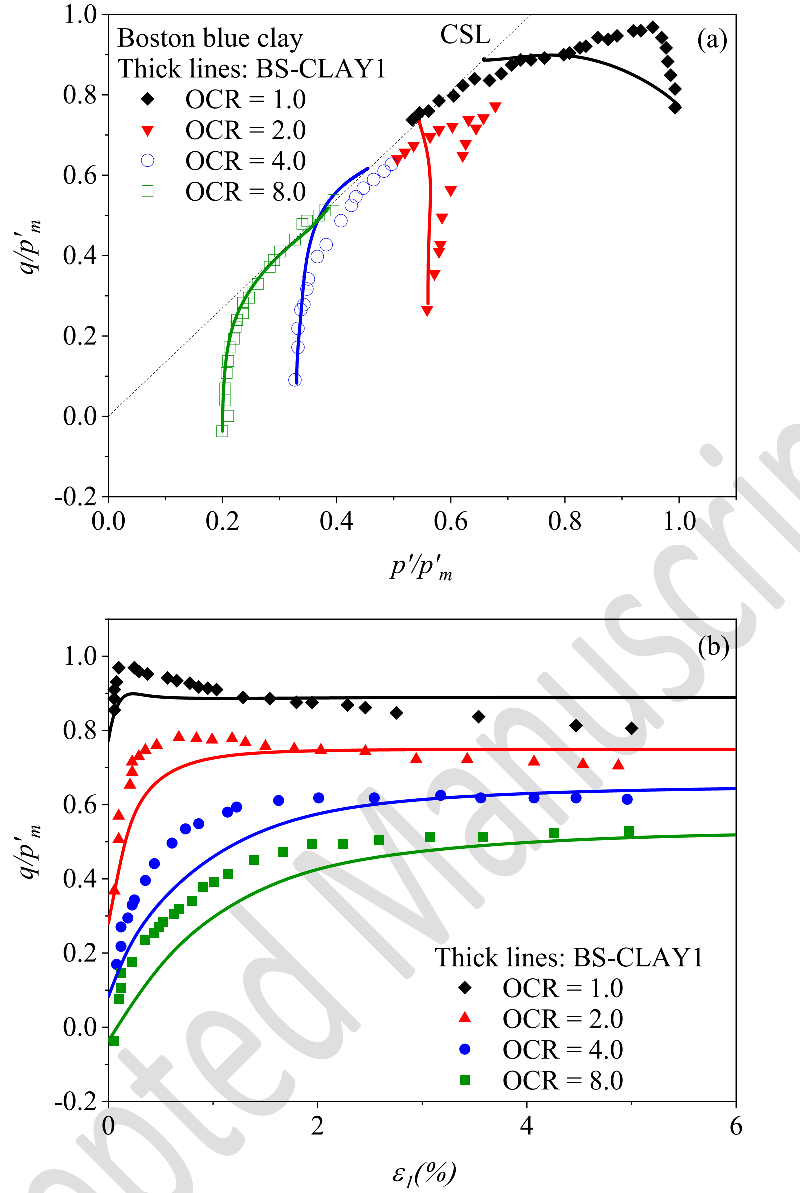

Fig. 11. Comparison of BS-CLAY1 predictions for Boston blue clay

6.3. Lower Cromer till

The compression triaxial tests on anisotropically consolidated samples of Lower Cromer till (Gens, 1982) are also used to evaluate the model performance. The low plasticity glacial till samples were obtained from the Norfolk coast in the UK where the deposit had been part of the North Sea Drift. This sandy clay has a liquid limit and a plastic limit of 25% and 13%, respectively. Gens (1982) performed his experiments on reconstituted samples which were taken from uniform specimens, and hence, the variability of this natural material was overlooked.

Fig. 12 shows the BS-CLAY1 predictions of undrained anisotropic shearing of Lower Cromer till samples corresponding to tests at different OCRs. Fig. 12a illustrates that for LOC and HOC samples the model predictions of anisotropic stress paths are qualitatively and quantitatively consistent with the experimental results. For the test at OCR=1, the model prediction has a notable difference with the test measurements, and the proposed model is unable to reproduce the softening behaviour, same as the simulations in Yang et al. (2015b). Moreover, similar to the case of Boston blue clay for the OCR=2, the model shows a poor simulation in stress space, while it has captured the failure strength in stress-strain space, properly. However, the proposed model shows promising performance in simulating the HOC samples.

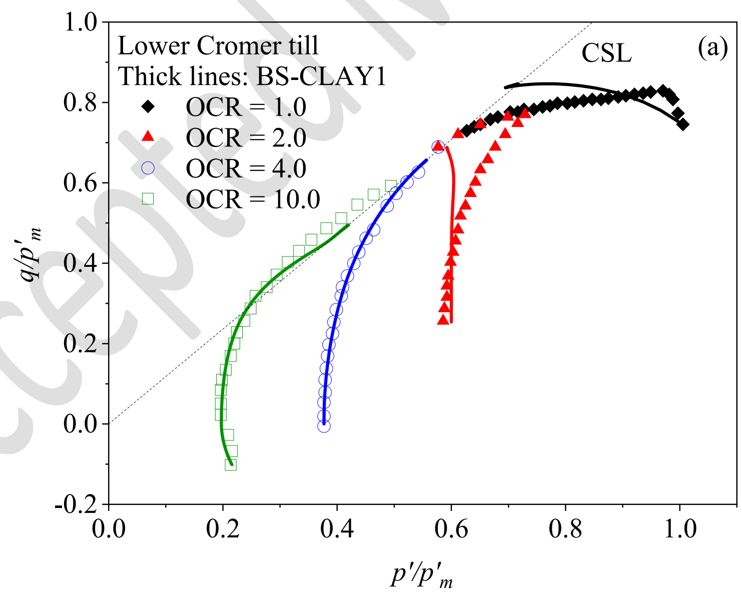

Computers and Geotechnics 135 (2021). Submitted 17 Sep 2020; Published 29 April 2021. https://doi.org/10.1016/j.compgeo.2021.104099.

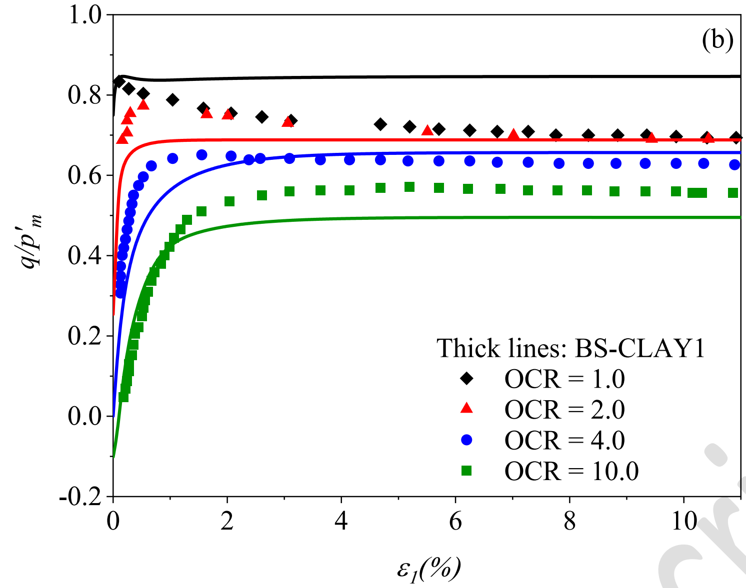

Fig. 12. Comparison of BS-CLAY1 predictions for Lower Cromer till

7. Conclusion

A new anisotropic constitutive model has been developed within the critical state based constitutive modeling framework. The new model is formulated based on a rotational hardening rule and the bounding surface plasticity concept to simultaneously capture the fabric anisotropy effects and the nonlinearity of soil responses before triggering the yield criterion. For the BS extension, a step-be-step novel framework is employed that enhanced the prediction capabilities of simple models with elliptical yield surfaces. The proposed framework is unique in its own way since in addition to capturing the nonlinear behaviour inside the BS, it produces desirable simulations for highly overconsolidated clays without the need to add more complications to the model (i.e. non-elliptical yield surface with additional parameters). The proposed framework includes a new modified method has been proposed to find the projection center which significantly improved the model performance for stiff clays. The second component of the proposed framework is a new concept to modify the BS configuration while the stress state varies within the BS. Moreover, to enhance the model capabilities in simulating the HOC samples, a non-associated flow rule is also adopted. The new model, BS-CLAY1, has six additional parameters compared to its preceding model, which only two of them need calibration through simulations of experimental data and the other four parameters can be determined using the provided relations using the value of OCR. The numerical implementation of the model was developed via an explicit Euler Forward integration scheme for the stress states inside the BS and an implicit Euler Backward integration scheme for the stress states on the BS. The model was then employed for prediction of the responses of three different anisotropically consolidated clayey soils at different OCRs. The comparison of model predictions against experimental data particularly illustrated the enhanced capabilities of the model in capturing the responses of LOC to HOC soils. Since the developments in this paper preserve some of the key original features of the S-CLAY1 model, there could be shortfalls in the accuracy of simulations in the cases of both stress path and stress-strain responses, particularly for normally consolidated (NC) samples. Although the adopted non-associated flow rule provides notably better predictions for tests over NC soils, employing a non-elliptical yield surface and developing a more flexible rotational hardening rule can address most of the deficiencies associated with simple elliptical models.

Acknowledgements

The financial support of the RFCS project MINRESCUE (Contract RFCS-RPJ-899518) funded by the European Commission is gratefully acknowledged.

Computers and Geotechnics 135 (2021). Submitted 17 Sep 2020; Published 29 April 2021. https://doi.org/10.1016/j.compgeo.2021.104099.

Appendix

The plastic modulus of the BS is achieved from consistency condition which requires that the stress state must remain on the BS during the plastic straining. The mathematical expression of the consistency condition is

$$\dot{F} = \frac{\partial F}{\partial \bar{\sigma}_{ij}} d\bar{\sigma}_{ij} + \frac{\partial F}{\partial \alpha_{ij}^{d}} d\alpha_{ij}^{d} + \frac{\partial F}{\partial \bar{p}'_m} d\bar{p}'_m = 0 \tag{1a}$$

which can be rewritten in the following form

$$\dot{F} = \frac{\partial F}{\partial \bar{\sigma}_{ij}} d\bar{\sigma}_{ij} + \frac{\partial F}{\partial \alpha_{ij}^{d}} d\alpha_{ij}^{d} + \frac{\partial F}{\partial \bar{p}'_m} \frac{d\bar{p}'_m}{d\varepsilon_v^p} d\varepsilon_v^p = 0 \tag{2a}$$

According to hardening rules (Eqs. (5), (6) and (7)), we have

$$\frac{d\bar{p}'_m}{d\varepsilon_v^p} = \frac{v\bar{p}'_m}{\lambda - \kappa} \tag{3a}$$

$$\begin{aligned} d\alpha_{ij}^{d} &= \mu\left(\left[\frac{3\bar{\sigma}_{ij}^{d}}{4\bar{p}'} - \alpha_{ij}^{d}\right]\langle d\varepsilon_v^p\rangle + \beta\left[\frac{\bar{\sigma}_{ij}^{d}}{3\bar{p}'} - \alpha_{ij}^{d}\right] d\varepsilon_d^p\right) \\ &= \mu\left(\left[\frac{3\bar{\sigma}_{ij}^{d}}{4\bar{p}'} - \alpha_{ij}^{d}\right] < \frac{1}{\bar{K}_p}\frac{\partial F}{\partial \bar{\sigma}_{kl}} d\bar{\sigma}_{kl} \frac{\partial G}{\partial \bar{p}'} \right. \\ &\quad \left. > +\beta\left[\frac{\bar{\sigma}_{ij}^{d}}{3\bar{p}'} - \alpha_{ij}^{d}\right]\frac{1}{\bar{K}_p}\frac{\partial F}{\partial \bar{\sigma}_{kl}} d\bar{\sigma}_{kl}\sqrt{\frac{2}{3}\left(\frac{\partial G}{\partial \bar{\sigma}_{mn}^{d}}\right)\left(\frac{\partial G}{\partial \bar{\sigma}_{mn}^{d}}\right)}\right) \end{aligned} \tag{4a}$$

Eqs. (4a) can be rewritten in the following form

$$d\alpha_{ij}^{d}=\left(\frac{\partial \alpha_{ij}^{d}}{\partial \varepsilon_{v}^{p}}<\frac{1}{\bar{K}_{p}}\frac{\partial F}{\partial \bar{\sigma}_{kl}}d\bar{\sigma}_{kl}\frac{\partial G}{\partial \bar{p}'}\right.$$

$$\left.>+\frac{\partial \alpha_{ij}^{d}}{\partial \varepsilon_{d}^{p}}\frac{1}{\bar{K}_{p}}\frac{\partial F}{\partial \bar{\sigma}_{kl}}d\bar{\sigma}_{kl}\sqrt{\frac{2}{3}\left(\frac{\partial G}{\partial \bar{\sigma}_{mn}^{d}}\right)\left(\frac{\partial G}{\partial \bar{\sigma}_{mn}^{d}}\right)}\right) \tag{5a}$$

Putting Eqs. (3a), and (5a) in the consistency condition, we have

$$\frac{\partial F}{\partial \bar{\sigma}_{ij}}d\bar{\sigma}_{ij}+\frac{\partial F}{\partial \alpha_{ij}^{d}}\left(\frac{\partial \alpha_{ij}^{d}}{\partial \varepsilon_{v}^{p}}<\frac{1}{\bar{K}_{p}}\frac{\partial F}{\partial \bar{\sigma}_{kl}}d\bar{\sigma}_{kl}\frac{\partial G}{\partial \bar{p}'}\right.$$

$$\left.>+\frac{\partial \alpha_{ij}^{d}}{\partial \varepsilon_{d}^{p}}\frac{1}{\bar{K}_{p}}\frac{\partial F}{\partial \bar{\sigma}_{kl}}d\bar{\sigma}_{kl}\sqrt{\frac{2}{3}\left(\frac{\partial G}{\partial \bar{\sigma}_{mn}^{d}}\right)\left(\frac{\partial G}{\partial \bar{\sigma}_{mn}^{d}}\right)}\right) \tag{6a}$$

$$+\frac{\delta F}{\delta \bar{p}_{m}'}\frac{\nu \bar{p}_{m}'}{\lambda-\kappa}\left(\frac{1}{\bar{K}_{p}}\frac{\partial F}{\partial \bar{\sigma}_{kl}}d\bar{\sigma}_{kl}\frac{\partial G}{\partial \bar{p}'}\right)=0$$

After some simplifications, the plastic modulus of bounding surface can be obtained as

$$\bar{K}_{p}=-\frac{\partial F}{\partial \alpha_{ij}^{d}}\left(\frac{\partial \alpha_{ij}^{d}}{\partial \varepsilon_{v}^{p}}\langle\frac{\partial G}{\partial \bar{p}'}\rangle+\frac{\partial \alpha_{ij}^{d}}{\partial \varepsilon_{d}^{p}}\sqrt{\frac{2}{3}\frac{\partial G}{\partial \bar{\sigma}_{ij}^{d}}\frac{\partial G}{\partial \bar{\sigma}_{ij}^{d}}}\right)-\frac{\partial F}{\partial \bar{p}_{m}'}\frac{\nu \bar{p}_{m}'}{\lambda-\kappa}\frac{\partial G}{\partial \bar{p}'} \tag{7a}$$

where the $\bar{K}_{p}$ is used besides the Eqs. (9) and (10) to determine the plastic modulus of the SS, and therefore, to calculate the elastoplastic stiffness tensor at the current SS.

References

Anandarajah, A., Dafalias, Y.F., 1986. Bounding surface plasticity. III: Application to anisotropic cohesive soils. J. Eng. Mech. 112 (12), 1292–1318.

Banerjee, P.K., Stipho, A.S., Yousif, N.B., 1985. A theoretical and experimental investigation of the behaviour of anisotropically consolidated clay. In: Developments in soil mechanics and foundation engineering, vol. 2. Cardiff University, pp. 1–41.

Banerjee, P.K., Yousif, N.B., 1986. A plasticity model for the mechanical behaviour of anisotropically consolidated clay. Int. J. Numer. Anal. Meth. Geomech. 10 (5), 521–541.

Chakraborty, T., Salgado, R., Loukidis, D., 2013. A two-surface plasticity model for clay. Comput. Geotech. 49, 170–190.

Chen, Y.N., Yang, Z.X., 2017. A family of improved yield surfaces and their application in modeling of isotropically over-consolidated clays. Comput. Geotech. 90, 133–143.

Chen, Y., Yang, Z., 2020. A bounding surface model for anisotropically overconsolidated clay incorporating thermodynamics admissible rotational hardening rule. Int. J. Numer. Anal. Meth. Geomech. 44 (5), 668–690.

Collins, I.F., Kelly, P.A., 2002. A thermomechanical analysis of a family of soil models. Geotechnique 52 (7), 507–518.

Collins, I.F., Hilder, T., 2002. A theoretical framework for constructing elastic/plastic constitutive models of triaxial tests. Int. J. Numer. Anal. Meth. Geomech. 26 (13), 1313–1347.

Coombs, W.M., 2017. Continuously unique anisotropic critical state hyperplasticity. Int. J. Numer. Anal. Meth. Geomech. 41 (4), 578–601.

Crouch, R.S., Wolf, J.P., Dafalias, Y.F., 1994. Unified critical-state bounding-surface plasticity model for soil. J. Eng. Mech. 120 (11), 2251–2270.

Dafalias, Y.F., 1986a. An anisotropic critical state soil plasticity model. Mech. Res. Commun. 13 (6), 341–347.

Dafalias, Y.F., Popov, E.P., 1975. A model of nonlinearly hardening materials for complex loading. Acta Mech. 21 (3), 173–192.

Dafalias, Y.F., Popov, E.P., 1976. Plastic internal variables formalism of cyclic plasticity. J. Appl. Mech. 43 (4), 645–651. https://doi.org/10.1115/1.3423948.

Dafalias, Y.F., Taiebat, M., 2013. Anatomy of rotational hardening in clay plasticity. Geotechnique 63 (16), 1406–1418.

Dafalias, Y.F., Taiebat, M., 2014. Rotational hardening with and without anisotropic fabric at critical state. Geotechnique 64 (6), 507–511.

Dafalias, Y.F., Taiebat, M., Rollo, F., Amorosi, A., 2020. Convergence of rotational hardening with bounds in clay plasticity. Geotechnique Lett. 10 (1), 16–19.

Dafalias, Y.F., 1986b. Bounding surface plasticity. I: Mathematical foundation and hypoplasticity. J. Eng. Mech. 112 (9), 966–987.

Dafalias, Y.F., Herrmann, L.R., 1986. Bounding surface plasticity. II: Application to isotropic cohesive soils. J. Eng. Mech. 112 (12), 1263–1291.

Dafalias, Y.F., Manzari, M.T., Papadimitriou, A.G., 2006. SANICLAY: Simple anisotropic clay plasticity model. Int. J. Numer. Anal. Meth. Geomech. 30 (12), 1231–1257.

Fayad, P., 1986. Aspects of the volumetric and undrained behavior of Boston Blue clay. MS thesis. Department of Civil Engineering, Massachusetts Institute of Technology, Cambridge.

Gens, A., 1982. Stress-strain and strength characteristics of a low plasticity clay. PhD thesis, Imperial College of London, London, UK.

Gens, A., Nova, R., 1993. Conceptual bases for a constitutive model for bonded soils and weak rocks. Proc. Int. Conf. Hard Soils - Soft Rocks 1, 485–494.

Graham, J., Noonan, M.L., Lew, K.V., 1983. Yield states and stress-strain relationships in a natural plastic clay. Can. Geotech. J. 20 (3), 502–516.

Hashiguchi, K., 1977. An expression of anisotropy in a plastic constitutive equation of soils (Disucssion of "Induced anisotropy and time dependency in clays"). Proc. 9th ICSMFE, Special Session 9, 302–305.

Jiang, J., Ling, H.I., Kaliakin, V.N., 2012. An associative and non-associative anisotropic bounding surface nodel for clay. J. Appl. Mech., Trans. ASME 79 (3).

Jiang, J., Ling, H.I., 2010. A framework of an anisotropic elastoplastic model for clays. Mech. Res. Commun. 37 (4), 394–398.

Karstunen, M., Krenn, H., Wheeler, S.J., Koskinen, M., Zentar, R., 2005. Effect of anisotropy and destructuration on the behavior of Murro test embankment. Int. J. Geomech. 5 (2), 87–97.

Karstunen, M., Rezania, M., Sivasithamparam, N., Yin, Z.Y., 2015. Comparison of anisotropic rate-dependent models for modeling consolidation of soft clays. Int. J. Geomech. 15 (5), A4014003.

Karstunen, M., Rezania, M., Sivasithamparam, N., 2013. Comparison of anisotropic rate-dependent models at element level. In: Springer Series in Geomechanics and Geoengineering. Springer, pp. 115–119.

Computers and Geotechnics 135 (2021). Submitted 17 Sep 2020; Published 29 April 2021. https://doi.org/10.1016/j.compgeo.2021.104099.

Ladd, C.C., Varallyay, J., 1965. The influence of stress system on the behaviour of saturated clays during undrained shear. Research Report No R65-11. Department of Civil Engineering, MIT, Cambridge, MA.

Krieg, R.D., 1975. Practical two surface plasticity theory. J. Appl. Mech. 42, 641–646.

Lagioia, R., Puzrin, A.M., Potts, D.M., 1996. A new versatile expression for yield and plastic potential surfaces. Comput. Geotech. 19 (3), 171–191.

Ling, H.I., Yue, D., Kaliakin, V.N., Themelis, N.J., 2002. Anisotropic elastoplastic bounding surface model for cohesive soils. J. Eng. Mech. 128 (7), 748–758.

Mayne, P.W., Kulhawy, F.H., 1982. K0- OCR relationships in soil. J. Geotech. Eng. Div., ASCE 108 (GT6), 851–872.

Nieto Leal, A., Kaliakin, V.N., Mashayekhi, M., 2018. Improved rotational hardening rule for cohesive soils and definition of inherent anisotropy. Int. J. Numer. Anal. Meth. Geomech. 42 (3), 469–487.

Nishimura, S., Minh, N.A., Jardine, R.J., 2007. Shear strength anisotropy of natural London Clay. Geotechnique 57 (1), 49–62.

Ottosen, N., Ristinmaa, M., 2005. The mechanics of constitutive modeling. In: The Mechanics of Constitutive Modeling. Elsevier.

Rezania, M., Bagheri, M., Mousavi Nezhad, M., Sivasithamparam, N., 2017a. Creep analysis of an earth embankment on soft soil deposit with and without PVD improvement. Geotext. Geomembr. 45 (5), 537–547.

Rezania, M., Mousavi Nezhad, M., Dejaloud, H., 2014. SCLAY1S-BS: An anisotropic model for simulation of cyclic behaviour of clays. In: Soga, K., Kumar, K., Biscontin, G., Kuo, M. (Eds.), Geomechanics from Micro to Macro. CRC Press, pp. 651–655.

Computers and Geotechnics 135 (2021). Submitted 17 Sep 2020; Published 29 April 2021. https://doi.org/10.1016/j.compgeo.2021.104099.

Rezania, M., Nezhad, M.M., Zanganeh, H., Castro, J., Sivasithamparam, N., 2017b. Modeling pile setup in natural clay deposit considering soil anisotropy, structure, and creep effects: Case study. Int. J. Geomech. 17 (3), 4016075.

Rezania, M., Nguyen, H., Zanganeh, H., Taiebat, M., 2018. Numerical analysis of Ballina test embankment on a soft structured clay foundation. Comput. Geotech. 93, 61–74.

Rezania, M., Sivasithamparam, N., Mousavi Nezhad, M., 2014. On the stress update algorithm of an advanced critical state elasto-plastic model and the effect of yield function equation. Finite Elem. Anal. Des. 90, 74–83.

Rezania, M., Taiebat, M., Poletti, E., 2016. A viscoplastic SANICLAY model for natural soft soils. Comput. Geotech. 73, 128–141.

Roscoe, K., Burland, J.B., 1968. On the generalized stress-strain behavior of "wet" clay. Engineering Plasticity. Cambridge University Press, pp. 535–609.

Seidalinov, G., Taiebat, M., 2014. Bounding surface SANICLAY plasticity model for cyclic clay behavior. Int. J. Numer. Anal. Meth. Geomech. 38 (7), 702–724.

Sekiguchi, H., Ohta, H., 1977. Induced Anisotropy and time dependancy in clays. In: Proc. 9th ICSMFE, pp. 163–175.

Sivasithamparam, N., Castro, J., 2016. An anisotropic elastoplastic model for soft clays based on logarithmic contractancy. Int. J. Numer. Anal. Meth. Geomech. 40 (4), 596–621.

Sivasithamparam, N., Karstunen, M., Bonnier, P., 2015. Modelling creep behaviour of anisotropic soft soils. Comput. Geotech. 69, 46–57.

Sivasithamparam, N., Rezania, M., 2017. The comparison of modelling inherent and evolving anisotropy on the behaviour of a full-scale embankment. Int. J. Geotech. Eng. 11 (4), 343–354.

Computers and Geotechnics 135 (2021). Submitted 17 Sep 2020; Published 29 April 2021. https://doi.org/10.1016/j.compgeo.2021.104099.

Stipho, A.S.A., 1978. Experimental and theoretical investigation of the behavior of anisotropically consolidated kaolin. PhD thesis. Univ. College, Cardiff, U.K.

Taiebat, M., Dafalias, Y.F., 2010. Simple yield surface expressions appropriate for soil plasticity. Int. J. Geomech. 10 (4), 161–169.

Wheeler, S.J., Karstunen, M., Naatanen, A., 1999. Anisotropic hardening model for normally consolidated soft clays. Numerical Models in Geomechanics. Proceedings of the 7th International Symposium, Graz, September 1999, 33–40.

Wheeler, S.J., Naatanen, A., Karstunen, M., Lojander, M., 2003. An anisotropic elastoplastic model for soft clays. Can. Geotech. J. 40 (2), 403–418.

Whittle, A.J., Kavvadas, M.J., 1994. Formulation of MIT-E3 constitutive model for overconsolidated clays. J. Geotech. Eng. 120 (1), 173–198.

Wood, D.M., 1990. In: Soil behaviour and critical state soil mechanics. Cambridge University Press.

Yang, C., Carter, J.P., Yu, S., 2015a. Comparison of model predictions of the anisotropic plasticity of Lower Cromer Till. Comput. Geotech. 69, 365–377.

Yang, C., Sheng, D., Carter, J.P., Sloan, S.W., 2015b. Modelling the plastic anisotropy of Lower Cromer Till. Comput. Geotech. 69, 22–37.

Yildiz, A., Karstunen, M., Krenn, H., 2009. Effect of anisotropy and destructuration on behavior of Haarajoki test embankment. Int. J. Geomech. 9 (4), 153–168.

Yu, H.S., 1998. CASM: a unified state parameter model for clay and sand. Int. J. Numer. Anal. Meth. Geomech. 22 (8), 621–653.

Computers and Geotechnics 135 (2021). Submitted 17 Sep 2020; Published 29 April 2021. https://doi.org/10.1016/j.compgeo.2021.104099.

Zentar, R., Karstunen, M., Wheeler, S.J., 2002. Influence of anisotropy and destructuration on undrained shearing of natural clays. In: Proceedings of the 5th European Conference on Numerical Methods in Geotechnical Engineering, pp. 21–26.

Zhou, C., Yin, J.H., Zhu, J.G., Cheng, C.M., 2005. Elastic anisotropic viscoplastic modeling of the strain-rate-dependent stress-strain behavior of K0-consolidated natural marine clays in triaxial shear tests. Int. J. Geomech. 5 (3), 218–232